Electronic Supplementary Information (ESI)

Short-Range Order in Defective Half-Heusler Thermoelectric Crystals

Kaiyang Xia,[a] Pengfei Nan,[b] Shihua Tan,[c] Yumei Wang,[b] Binghui Ge,[bd] Wenqing Zhang, [c] Shashwat Anand,[e] Xinbing Zhao,[a] G. Jeffrey Snyder,[e] and Tiejun Zhu[a]

[a] State Key laboratory of Silicon Materials, School of Materials Science and Engineering, Zhejiang University, Hangzhou 310027, China.

[b] Beijing National Laboratory for Condensed Matter Physics, Institute of Physics, Chinese Academy of Sciences, Beijing 100190, China.

[c] Shenzhen Key Laboratory of Thermoelectric Materials and Department of Physics, Southern University of Science and Technology, Shenzhen 518055, China

[d] Institute of Physics Science and Information Technology, Anhui University, Hefei 230601, China.

[e] Department of Materials Science and Engineering, Northwestern University, Evanston IL 60208, USA.

‡ These authors contributed equally.

* Email: zhutj@zju.edu.cn

Supplementary Information

Methods

Sample Preparation

The samples were fabricated by levitation melting and spark plasma sintering (SPS). Ingots (~15 g) were prepared by levitation melting of stoichiometric amounts of elements Nb (foil, 3N), Co (piece, 4N), Sb (block, 5N), V (piece, 3N), Ti (rod, 4N), Ni (piece, 4N) under an argon atmosphere, and the melt was quenched in a water-cooled copper crucible. Melting was carried out thrice to ensure homogeneity. The resulting ingots were then mechanically milled (Mixer Mill MM200, Retsch) with an oscillation frequency of 24 Hz for 1 hour under argon protection. The obtained powders were sintered by SPS (LABOX-650F, SINTER LAND INC.) around 1173 K under 65 MPa in a vacuum for 10 min. The density ρ was measured by Archimedes method, and the relative density of the pure phase samples was found to be ~98%.

Sample Characterization

XRD was performed on a RigakuD/MAX-2550PC diffractometer with Cu K_α radiation. XPS was performed on a Kratos Axis Supra after the sputtering process for 1 min to remove the oxide layer on the sample surface. TEM investigations were carried out by JEM-ARM200F with double Cs corrector. The samples for TEM observation were prepared by mechanical polishing, dimpling and ion milling with liquid nitrogen. To verify the existence of diffuse bands, samples was cleaned again, in the low energy with ion milling, to clear damaged layers on the surface to avoid the surface effect.

Thermoelectric Measurement

The room temperature Hall coefficient was measured in a Mini Cryogen Free Measurement System (Cryogenic Limited, UK) under a variable magnetic field of $\pm$ 4 T. The carrier concentration n_H was calculated by $n_H = 1/eR_H$, where e is the unit charge and R_H is the Hall coefficient. The estimated error of Hall coefficient is within $\pm 10\%$. The Seebeck coefficient and the electrical conductivity from 300-1123 K were measured on a commercial Linseis LSR-3 system using a differential voltage/ temperature technique and a DC four-probe method. The accuracy is $\pm 5\%$ and $\pm 3\%$, respectively. The thermal conductivity κ was then calculated by $\kappa = D\rho C_p$. The thermal diffusivity D was measured using the laser flash method (Netzsch, LFA457) and the accuracy is $\pm 3\%$. The heat capacity C_p was rationally calculated by the equation $C_p = C_{ph,H} + C_D$, where $C_{ph,H}$ is the harmonic term of phonon contribution and C_D is the thermal expansion term for heat capacity, which can be calculated by sound velocity, thermal expansion coefficient and density.[1] Normal and shear ultrasonic measurements were performed at room temperature using input from a Panametrics 5052 pulser/receiver with the filter at 0.03 MHz. The response was recorded via a Tektronic TDS5054B-NV digital oscilloscope. The thermal expansion coefficient was measured by Netzsch DIL 402 PC. The κ_L was calculated by subtracting the κ_e from the κ. κ_e was calculated by the Wiedemann–Franz law ($\kappa_e = \sigma LT$), and the Lorenz number L was calculated using the SPB model and the measured Seebeck coefficient.[2] The κ and L for $Nb_{0.8}Co_{1-x}Ni_xSb$ ($x = 0$-0.10) are shown in Fig. S8 (ESI†).

Monte Carlo Simulations

The Cluster Expansion (CE) method is used to simulate the large systems that cannot be directly calculated by DFT. Our CE relied on a basis set of pair interactions up to the 4th nearest neighbor (4th-NN, two lattice sites), triplet (three sites) and quadruplet (four sites) interactions up to 2nd-NN, with respect to a rocksalt primitive cell with lattice constant a = 4.192 Å found by DFT calculation with all lattice and atom positions fully relaxed (up to 56 atoms).[3] The DFT energies of 17 lattice-fixed structures (most of them are $(Nb_{0.8}CoSb)_n$), which contain all possible occupations in the above-mentioned basis set, is used to fit the effective cluster interactions in CE Hamiltonians. Our CE model was found to reproduce DFT energies of $(Nb_{0.8}CoSb)_n$ with good accuracy (<10meV per Nb site). The root mean square error between CE energy and DFT energy of 88 out-of-sample lattice-fixed structures is less than 9meV per Nb-site. All canonical Monte Carlo (MC) simulations based on these CE Hamiltonians were performed using the Alloy Theoretic Automated Toolkit (ATAT).[4, 5] Each MC structure contains 27000 Nb-sites, of which 5400 are occupied by vacancy (Vac).

Estimation of ☐ L

A simplified model based on the Debye approximation was adopted to estimate the phonon transport mechanism. The lattice thermal conductivity is given by[6]

$$\kappa_{\mathrm{L}} = \frac{k_{\mathrm{B}}}{2\pi^2 v_{\mathrm{s}}} (\frac{k_{\mathrm{B}}T}{\hbar})^3 \int\limits_0^{\theta_{\mathrm{D}}/T} \tau(x) \frac{x^4 e^x}{(e^x - 1)^2} dx \qquad (S1)$$

where $x = \hbar\omega/k_{\mathrm{B}}T$ is the reduced phonon frequency; k_{B} is the Boltzmann constant; $\hbar$ is the reduced Planck constant; θ_{D} is the Debye temperature; v_{s} is the sound velocity; and τ is the effective relaxation time, which can be calculated via Matthiessen's rule $\tau^{-1} = \Sigma \, \tau_{\mathrm{i}}^1$. In thermoelectrics, Umklapp scattering (U), point defect scattering (PD), electron-phonon scattering (EP) and boundary scattering (B) are common and important mechanisms of phonon scattering, and the effective relaxation time τ can be described as

$$\tau^{-1} = A\omega^2 T \exp(-\theta_{\mathrm{D}}/3T) + B\omega^4 + C\omega^2 + v_s/d \qquad (S2)$$

where d is the grain size and v_s/d represents the probability of boundary scattering. A, B and C are three prefactor of for U, PD and EP scattering relaxation time, respectively. In the case of the $Nb_{0.8}CoSb$, the decrease of lattice thermal conductivity caused by intrinsic Nb vacancies should be essential. The prefactor B of point defect scattering is given by

$$B = \frac{V_0}{4\pi v_s^3} \Gamma = \frac{V_0}{4\pi v_s^3} (\Gamma_{\mathrm{M}} + \Gamma_{\mathrm{S}}) \qquad (S3)$$

where V_0 is the volume of the primitive cell, and Γ is the disorder scattering parameter. Phonon scattering due to point defect mainly comes from the combined effects of the mass and strain disorders, which can be characterized by Γ_{M} and Γ_{S}, respectively. Considering the almost identified lattice parameters in $Nb_{0.8+\delta}CoSb$, we only calculated Γ_{M} between Nb atoms and vacancies, and assumed Nb sites is totally disordered for simplicity. The detailed calculation of point defects scattering can be found elsewhere.[7] Thus, the boundary scattering and point defects scattering relaxation times can be calculated independently. U scattering and electron-phonon scattering can be obtained by fitting the experimental data. The fitting line will deviate from the experimental values anyway if we take EP out of consideration, indicating the neglectable impact

of electron-phonon scattering on phonon transport in this system. The parameters used for the calculation are listed in Table S1. A good agreement between the experimental data and the calculated curves is reached (Fig. S1).

Table S1. Parameters used for estimate of κ_L for Nb$_{0.8}$CoSb

Scattering type	Parameter	Value
Umklapp scattering	A (10^{-18} s/K)	3.3
Point defects scattering	B (10^{-42} s^3)	2.39
	Sound velocity v_s (m/s)	3312
	Debye temperature θ_D (K)	385
Boundary scattering	Average grain size d (nm)	800
Electron-phonon scattering	C (10^{-16} s)	4.5

Supplementary Information Figures
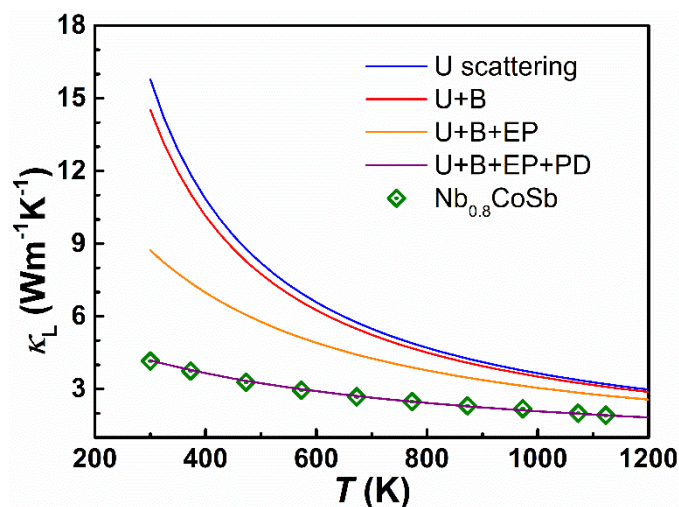
Fig. S1 Comparison of the experimental and calculated lattice thermal conductivities in the whole temperature region. The experimental data are from our previous work.[7] U, B, Ep and PD denote the Umklapp process, boundary, electron-phonon and point defect scattering, respectively.
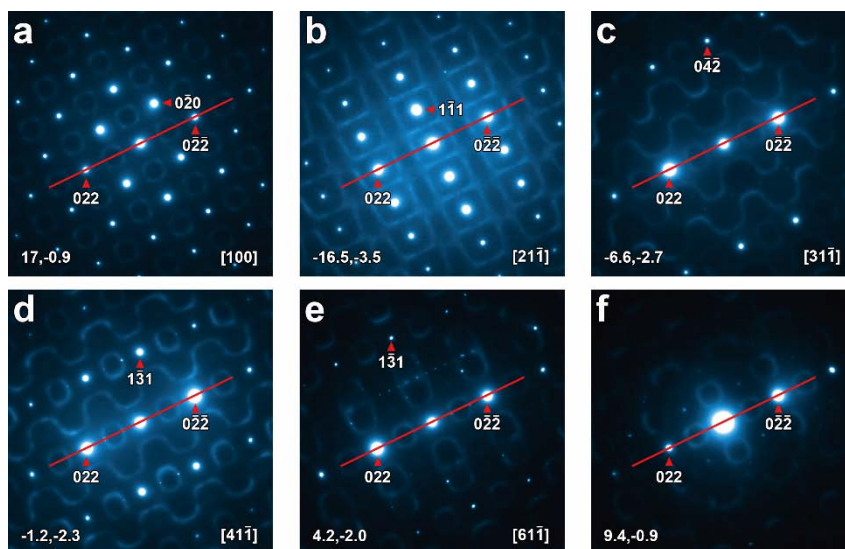

Fig. S2 Tilt series diffraction patterns of $Nb_{0.8}CoSb$ in (a) [1 0 0], (b) [2 1 -1], (c) [3 1 -1], (d) [4 1 -1], (e) [6 1 -1] direction and (f) between [1 0 0] and [6 1 -1] direction.

We tilted the TEM sample from the orientation of [100] with the 022 direction as an axis, then we got [2 1 -1], [3 1 -1], [4 1 -1] and [6 1 -1] electron diffraction patterns successively with the corresponding tilting angle inset in Figure S1. Besides these diffraction patterns, the last diffraction pattern is between [1 0 0] and [6 1 -1] direction, and deviates from any zone axis, then it will eliminate the contribution of the dynamical effect and still shows the diffuse bands, which indicate the diffuse band is an intrinsic characterization of this material.
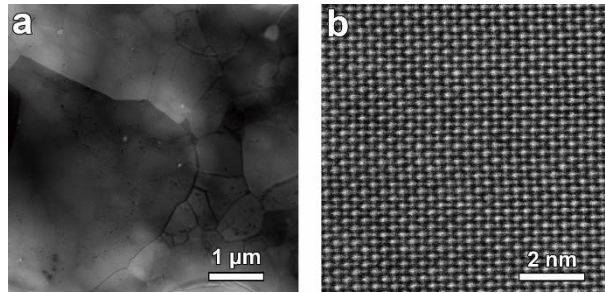
Fig. S3 (a) Transmission electron microscope image of Nb0.8CoSb sample. No obvious dense dislocation can be found. (b) High-resolution transmission electron microscope image of Nb0.8CoSb sample in [1 0 0] direction.
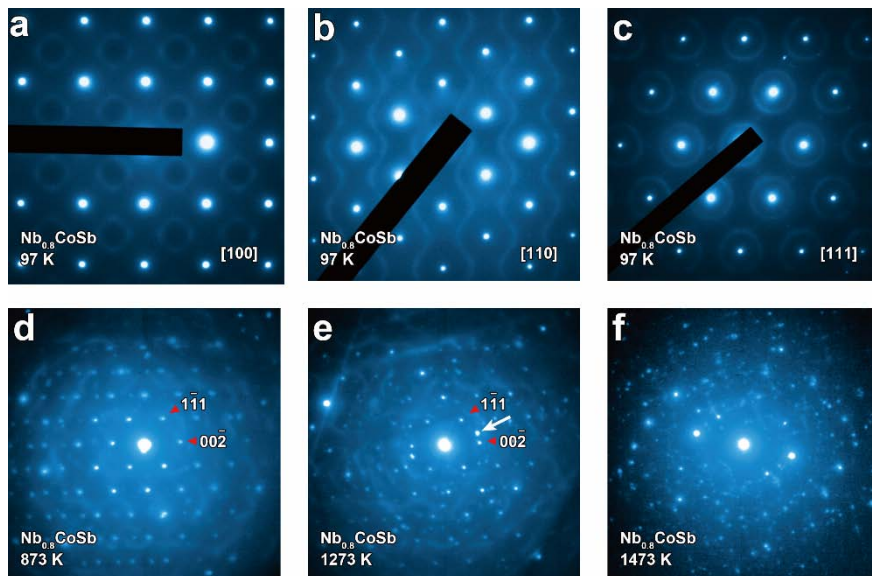

Fig. S4 Cooling test at 97 K in (a) [1 0 0], (b) [1 1 0], (c) [1 1 1] direction, and heating test at (d) 873 K, (e) 1273 K and (f) 1473 K of Nb0.8CoSb in [1 1 0] direction.

Cooling test was carried out from room temperature to 96 K, and the diffuse bands can be observe during the whole process. Heating test was carried out from room temperature to 1473 K. The sample is stable during the heating process until 1273 K, at which a new diffraction spot appears, denoted by a white arrow in Fig. S3e, and indicates a new phase was formed.
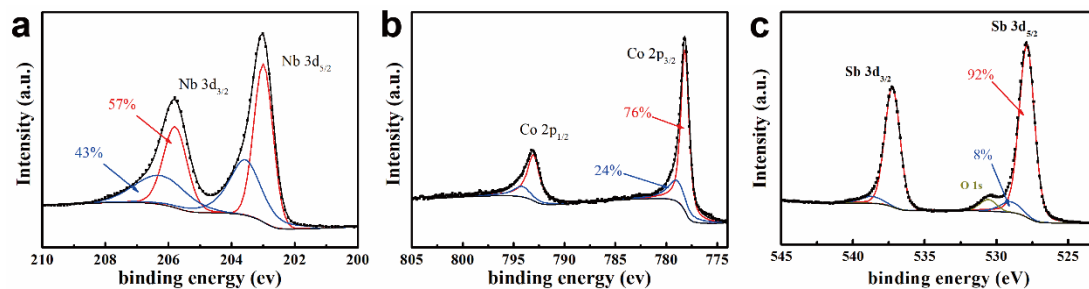

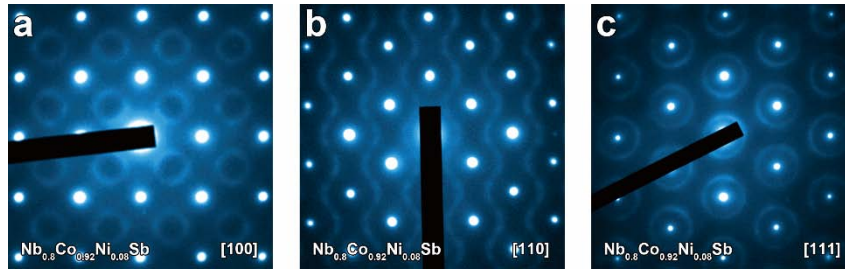**Fig. S5** XPS spectra of (a) Nb 3d, (b) Co 2p and (c) Sb 3d in $Nb_{0.8}CoSb$

Fig. S6 Diffraction patterns of $Nb_{0.8}Co_{0.92}Ni_{0.08}Sb$ in (a) [1 0 0], (b) [1 1 0] and (c) [1 1 1] direction. Only the fundamental diffraction spots together with circular-like or wavy diffuse bands can be obsereved, similar to those of $Nb_{0.8}CoSb$, indicating that Ni doping does not change the short-range order.

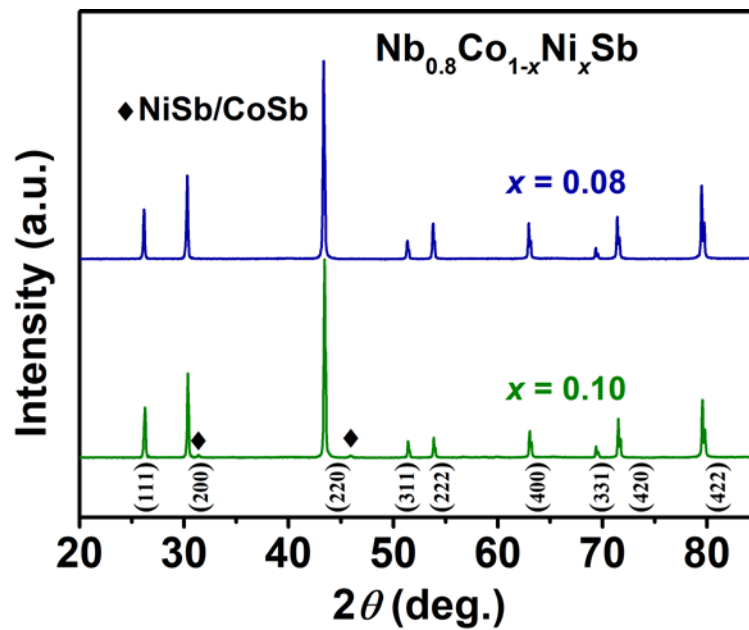**Fig. S7** Powder X-ray diffraction patterns of $Nb_{0.8}Co_{0.92}Ni_{0.08}Sb$ and $Nb_{0.8}Co_{0.90}Ni_{0.10}Sb$.
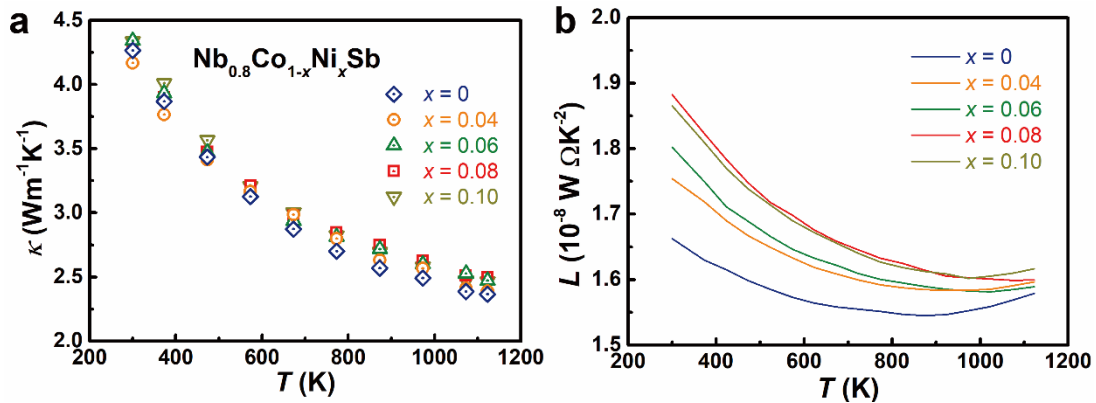
Fig. S8 Temperature dependence of (a) thermal conductivity κ, and (b) Lorenz number L for $Nb_{0.8}Co_{1-x}Ni_xSb$ (x = 0, 0.04, 0.06 and 0.08)

References

1. O. Delaire, A. F. May, M. A. McGuire, W. D. Porter, M. S. Lucas, M. B. Stone, D. L. Abernathy, V. A. Ravi, S. A. Firdosy and G. J. Snyder, *Phys. Rev. B*, 2009, **80**, 184302.

2. H. H. Xie, H. Wang, C. G. Fu, Y. T. Liu, G. J. Snyder, X. B. Zhao and T. J. Zhu, *Sci. Rep.*, 2014, **4**, 6888.

3. W. G. Zeier, S. Anand, L. H. Huang, R. He, H. Zhang, Z. F. Ren, C. Wolverton and G. J. Snyder, *Chem. Mater.*, 2017, **29**, 1210-1217.

4. J. Yang, G. P. Meisner, L. Chen, *Appl. Phys. Lett.* **2004**, *85*, 1140.

5. A. van de Walle, M. Asta and G. Ceder, *Calphad*, 2002, **26**, 539-553.

6. A. van de Walle and M. Asta, *Modelling Simul. Mater. Sci. Eng.*, 2002, **10**, 521-538.

7. K. Y. Xia, Y. T. Liu, S. Anand, G. J. Snyder, J. Z. Xin, J. J. Yu, X. B. Zhao and T. J. Zhu, *Adv. Funct. Mater.*, 2018, **28**, 1705845.